# The grating decomposition method: A new approach for understanding polarization-selective transient grating experiments. II. Applications

John T. Fourkas[a)]
*Department of Chemistry, Stanford University, Stanford, California 94305*

Rick Trebino[b)]
*Combustion Research Facility, Sandia National Laboratories, Livermore, California 94551*

M. D. Fayer
*Department of Chemistry, Stanford University, Stanford, California 94305*

(Received 2 August 1991; accepted 16 March 1992)

We apply the theory developed in Paper I to two transient grating problems that present difficulties in interpretation and/or calculation. The first application is general, and illustrates the ability of the grating decomposition method (GDM) to facilitate calculations and to provide intuition and insight in complex orientational grating experiments: we apply the GDM to nuclear optical Kerr effect (OKE) polarization gratings. We show that the circularly polarized component gratings of the polarization-grating decomposition do not contribute to the signal, and that the OKE polarization grating can therefore be viewed as the sum of two gratings with orthogonal net molecular alignments. We also use the GDM and this system to explain why polarization gratings can rotate the polarization of the probe beam. The second example is a detailed application of the GDM to an experiment in which the data cannot be fully interpreted using standard diagrammatic perturbation methods: picosecond transient gratings on the $D$ lines of gas-phase sodium atoms. We use the GDM and effective two-interaction matrix elements to greatly simplify this problem. We show why, in atmospheric-pressure experiments, Na intensity-grating decays are dominated by excited-state quenching, whereas Na polarization-grating decays are not. We show that the polarization-grating decays are dominated by Na diffusion and are influenced by scattering among the ground-state magnetic sublevels, but are unaffected by excited-state decay. We further show why the envelopes of polarization decays do not match the corresponding intensity-grating decays at large fringe spacings in low-pressure Na cells.

## I. INTRODUCTION

In the previous paper (hereafter referred to as I),[1] we developed the theory of the grating decomposition method (GDM) and effective two-interaction matrix elements (ETIMEs). We demonstrated that a polarization grating (i.e., a grating in which the excitation beams are of orthogonal linear polarizations) can be viewed at the third-order polarization level as the sum of four intensity gratings (gratings that are created by excitation beams of the same polarization). The polarization-grating decomposition consists of a right circularly polarized (RCP) intensity grating, an intensity grating that is $m$ polarized (i.e., linear at $-45°$) and is spatially $\pi/2$ radians out of phase with the RCP grating, an intensity grating that is left circularly polarized (LCP) and is spatially $\pi$ radians out of phase with the RCP grating, and an intensity grating that is $p$ polarized ($+45°$ linear) and is spatially $3\pi/2$ radians out of phase with the RCP grating. We will show here, in two examples, how the GDM and ETIMEs can be used to simplify orientational transient grating (TG) calculations and to provide important insight that is often not readily available in standard perturbative ($\chi^{(3)}$) approaches to orientational grating problems.

One of the problems, gratings formed by exciting the $D$ lines of gas-phase sodium atoms, cannot easily be treated fully and properly with standard diagrammatic perturbation theory (DPT). In atmospheric-pressure flames seeded with Na, intensity gratings decay at the Na excited-state collisional quenching rate, whereas polarization gratings decay much more slowly and are unaffected by excited-state quenching.[2,3] In low-pressure gas cells, the decays of Na intensity gratings are smooth and are affected by both excited-state decay and the transport of Na atoms. On the other hand, the decays of polarization gratings are dominated by Na transport and exhibit beats at the ground-state hyperfine-splitting frequency.[4,5] In addition, the envelope of the polarization-grating decays differs from the intensity-grating decays at fringe spacings large enough that the excited-state lifetime contribution to the decay is not negligible compared to the contribution from Na transport.

Modeling these experiments with standard DPT involves calculations that can be quite complicated. Furthermore, although the standard DPT treatment predicts the smooth decay of the intensity grating and the oscillations in the decay of the polarization grating, it does not provide a means of distinguishing the phenomenological damping

a) Present address: Department of Chemistry and Biochemistry, University of Texas at Austin, Austin, TX 78712.

b) Supported by the U.S. Department of Energy, Office of Basic Energy Sciences, Chemical Sciences Division.

 0021-9606/92/130078-08$06.00 

constants for these gratings. Here we present a detailed account of the application of the GDM and ETIMEs to this problem. We show that the GDM and ETIMEs, by readily allowing for the inclusion of spatial information, provide a complete explanation of the behavior of Na intensity and polarization gratings in both low-pressure gases and in flames, and greatly reduce the complexity of this calculation.

Before we consider this detailed example, we apply the GDM to a more general problem: nuclear optical Kerr effect orientational gratings. Although this problem has been treated previously,[6,7] we use the GDM and ETIMEs to simplify and add insight to its treatment.

## II. NUCLEAR OPTICAL KERR EFFECT GRATINGS

When liquid or gas molecules are exposed to an electric field, they tend to reorient in order to minimize the energy of the interaction with the field. The reorientation causes a net alignment in the medium, thereby producing a birefringence; this process is called the Kerr effect.[8] The optical Kerr effect (OKE) arises from the induced-dipole moments created in atoms and molecules by strong light fields, and has both an electronic and a nuclear component. The electronic OKE ($e$-OKE) is a change in the shape of the electron clouds of the atoms or molecules, and it decays essentially instantaneously when the light field is removed. On the other hand, the nuclear OKE ($n$-OKE) involves rotations of molecules, and it therefore generally decays much more slowly than the $e$-OKE.

The effect of OKE-induced birefringence on a grating signal can be calculated directly from the change in the index of refraction of the medium[6,9] or by using the symmetry properties of the nonlinear susceptibility tensor.[7,10] While the latter method is a powerful one that allows for the design of experiments that can separate, for instance, $n$- and $e$-OKE TG responses, it is somewhat lacking in physical insight. In addition, the susceptibility tensor elements can be derived directly from the birefringence calculation, and so the two approaches are ultimately equivalent. For the sake of clarity, we will use the first approach in combination with the GDM in deriving our results for OKE polarization gratings.

Following the notation of Sala and Richardson,[9] the OKE-induced birefringence is given by

$$\Delta n = \Delta n_{\parallel} - \Delta n_{\perp}, \tag{1}$$

where $\Delta n_{\parallel}$ and $\Delta n_{\perp}$ are the changes in the index of refraction for the polarizations parallel and perpendicular to the incident $e$ field. The components of the index of refraction parallel and perpendicular to the polarization of the light field are both influenced by the $e$- and $n$-OKE. We can write, in general,

$$\Delta n_{\parallel} = An_e + Bn_n \tag{2a}$$

and

$$\Delta n_{\perp} = (A-1)n_e + (B-1)n_n, \tag{2b}$$

where $n_e$ and $n_n$ are the $e$- and $n$-OKE contributions to the birefringence; they follow the relation

$$\Delta n = n_e + n_n. \tag{3}$$

Sala and Richardson showed that, under the circumstances in which most TG OKE experiments are performed, $A = 3/2$ and $B = 2/3$. We will use this value of $B$ in our treatment of this problem, although any values of $A$ or $B$ will give equivalent results in the GDM picture.

Both the $e$- and $n$-OKE can be probed using transient gratings, since the strength of the OKE is proportional to the amplitude of the light field that causes it. As mentioned above, the $e$-OKE tracks the laser pulses, whereas the $n$-OKE can provide important information about molecular motions; therefore, the $n$-OKE will be discussed here, although a similar treatment can be applied to the $e$-OKE.

Intensity and polarization gratings can both be used to study the $n$-OKE. It can be seen, from the intensity-grating electric-field picture, how the $n$-OKE contributes to the grating signal when the excitation beams are of the same polarization. The greatest molecular alignment (and therefore the greatest birefringence) occurs in the regions of the grating in which the electric field is strongest; thus, a birefringence grating is formed. As molecules undergo rotational diffusion, $\Delta n_{\parallel}$ and $\Delta n_{\perp}$ equalize, and $\Delta n$, which gives rise to the signal, goes to zero. The problem with using parallel-polarized excitation beams to study the OKE, however, is that interfering thermal and acoustic gratings are readily formed, even if there is only weak (e.g., vibrational overtone) absorption[11-14] or weak stimulated Brillouin scattering.[15]

Cross-polarized excitation beams remove both of these problems, since the excitation is of constant amplitude across the grating. On the other hand, it is not immediately obvious from the electric-field picture how the $n$-OKE produces a polarization-grating signal. We now describe a picture of orientational OKE gratings that follows directly from the GDM. Because the OKE must necessarily be describable by expressions such as Eq. (1) of I,[16] any picture based on the GDM is rigorously correct at third order. The contributions from the circularly polarized component gratings in the polarization-grating decomposition cancel one another, just as they do in absorption and emission gratings in isotropic molecular liquids. We can see this by replacing transition-dipole moments with polarizability vectors in the argument given for absorption and emission gratings in the argument in Sec. V of I. *Thus,* $\{\mathbf{x},\mathbf{y}^*\} = \{\mathbf{y},\mathbf{x}^*\}$ *for the n-OKE.*

We are left with two fully sinusoidal, linear intensity gratings, one $p$ polarized and one $m$ polarized [see Fig. 1(a)]. Each of these component gratings causes no net molecular alignment at its minima, and maximum alignment at its maxima, so the spatial dependences of contributions from the gratings are $1 + \sin(2\pi z/d)$ and $1 - \sin(2\pi z/d)$, respectively. We break up the probe beam into its $p$- and $m$-polarized components. The spatial index of refraction experienced by the components is given by

$$\begin{aligned} n(\mathbf{p}) &= n_0 + n_n\{\tfrac{2}{3}[1 + \sin(2\pi z/d)] \\ &\quad - \tfrac{1}{3}[1 - \sin(2\pi z/d)]\} \\ &= n_0 + n_n\left[\tfrac{1}{3} + \sin(2\pi z/d)\right] \end{aligned} \tag{4a}$$

and

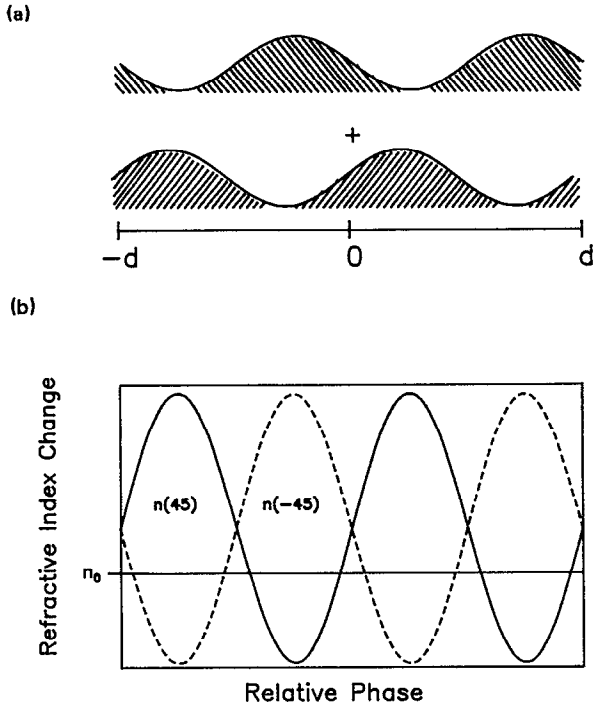


FIG. 1. (a) Molecular alignment in a nuclear optical Kerr effect polarization grating as predicted by the GDM. The net alignment is expressed as the sum of two fully sinusoidal gratings, one with + 45° alignment and one with − 45° alignment. (b) Spatial dependence of index of refraction change for $p$-polarized light (solid line) and for $m$-polarized light (dashed line), based on the model in (a).

$$n(\mathbf{m}) = n_0 + n_n\{-\tfrac{1}{3}[1+\sin(2\pi z/d)] + \tfrac{2}{3}[1-\sin(2\pi z/d)]\} = n_0 + n_n[\tfrac{1}{3}+\sin(2\pi z/d)], \quad (4b)$$

where $n_0$ is the index of refraction in the absence of an electric field. These expressions are plotted in Fig. 1(b). Within the framework of the GDM, the $n$-OKE polarization grating can be viewed as two-component linear intensity gratings that are 180° out of phase with one another. In one grating the molecules tend to be oriented in the **p** direction, whereas in the other grating the molecules tend to be oriented in the **m** direction. Furthermore, the same behavior is expected for the spatial dependence of the index of refraction of the **p** and **m** components of the probe polarization no matter what value $B$ takes on.

We can see readily from this analysis why a polarization grating can rotate the polarization of the probe beam: the $p$-polarized component of the probe beam sees a grating that is spatially shifted by 180° from the grating seen by the $m$-polarized component. Thus, there is a corresponding 180° spatial phase shift between the $p$-polarized and $m$-polarized components of the signal beam. A probe beam of polarization angle $45° + \theta$ therefore produces a signal beam at a polarization angle of $45° - \theta$; e.g., an $x$-polarized $[\sqrt{1/2}(\mathbf{p}+\mathbf{m})]$ probe beam produces a $y$-polarized $[\sqrt{1/2}(\mathbf{p}-\mathbf{m})]$ signal beam, and vice versa. By splitting up the probe into $r$- and $l$-polarized components, we can make a similar argument about probe beam rotation for systems in which the circularly polarized component gratings contribute to the signal.

Finally, we note that this treatment resolves inconsistencies in Eyring and Fayer's treatment of $n$-OKE polarization gratings;[6] their treatment led to the prediction of a discontinuity in the derivative of the spatial dependence of the index of refraction in the $n$-OKE polarization grating, which in turn leads to the prediction of higher-order diffraction at arbitrarily low laser intensities.[17] While the present analysis does not change past interpretations of time-dependent OKE TG data, it puts the experiments on a rigorous physical footing and augments the susceptibility tensor element symmetry approach to OKE transient gratings.

## III. GAS-PHASE Na GRATINGS

It is possible to model the systems in the previous example well enough to analyze data without using the GDM, although the GDM is valuable in adding insight to and simplifying the problem (as well as resolving inconsistencies in previous treatments). We now present a specific example of a set of experiments that are difficult to describe completely strictly within the confines of standard DPT: TG experiments atmospheric-pressure Na-seeded flames and in low-pressure Na vapor. Although there have been a substantial number of Na experiments described with DPT,[18–21] we show that the GDM and ETIMEs not only greatly simplify the treatment of these grating problems, but also readily provide spatial information that is essential to the understanding of the decay mechanisms involved.

Intensity- and polarization-grating experiments have been performed in the time domain in both Na-seeded flames[2,3] and low-pressure gas cells;[4,5] in addition, frequency-domain intensity and polarization-grating experiments have been performed in flames by Trebino and Rahn[20,21] and in sodium/buffer gas cells by Rotherberg and Bloembergen.[18,19] Whereas the intensity-grating data in each of the time-domain experiments can be explained readily using standard DPT, the interpretation of the polarization-grating data is not so straightforward. The difficulty in the interpretation of these data arises from the fact that different Na ground-state magnetic sublevels exhibit different spatial behavior in a polarization grating; this in turn affects the grating decay. We will use the properties of the Na ETIMEs to show that only the circularly polarized component gratings of the polarization grating need be considered. In addition, we will show that the contributions of the circularly polarized gratings to $\wp^{(3)}$ are identical when the 180° spatial phase shift between them is considered. Thus, the entire polarization-grating calculation can be reduced to a single circular intensity-grating calculation. Finally, with the aid of the GDM we will calculate the population depletion in each ground-state magnetic sublevel in the intensity and polarization gratings, and describe qualitatively how the differences in population transfer between the two types of grating account for the differences between the Na intensity- and polarization-grating decays in both flames and low-pressure cells.

Figures 2(a) and 2(b) show intensity- and polarization-

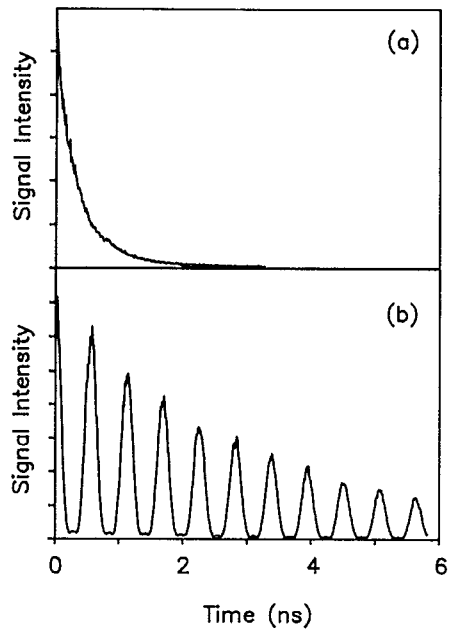


FIG. 2. (a) Linear intensity grating in a sodium-seeded, premixed, methane/air flame. The fringe spacing is 13.6 $\mu$m, the excitation wavelength 589.0 nm, and the probe wavelength 589.6 nm. (b) Polarization grating in the same flame under the same conditions. The oscillations in (b) are due to the Na ground-state hyperfine splitting. Note that the envelopes of the two decays are very different; (a) decays almost an order of magnitude faster than (b).

grating decays in a Na-seeded, premixed, methane-air flame at atmospheric pressure. At this high pressure, the mean free path of a Na atom is much smaller than the fringe spacing at which the data were taken; therefore, the Na transport is diffusive. The intensity-grating signal is given by[2,3,5]

$$S(t) \propto \exp(-2\Delta^2 Dt)\exp(-2t/\tau), \qquad (5)$$

where $D$ is the Na diffusion constant, $\Delta$ is $2\pi$ over the grating fringe spacing ($d$), $t$ is the probe delay time, and $\tau$ is the Na excited-state lifetime (16 ns in the absence of collisions[22]). Due to the presence of large concentrations of efficient Na excited-state quenchers (such as[23] $N_2$ and $CO_2$), the effective Na lifetime is expected to be much shorter than 16 ns in a fuel/air flame. This quenching should dominate the decay at large fringe spacings.[2,3] The intensity-grating decay is indeed exponential and is relatively insensitive to fringe spacing for medium to large fringe spacings. The polarization-grating data display large oscillations at the ground-state hyperfine-splitting frequency ($\omega_{hf}$), and the decay envelope is exponential. Surprisingly, however, the envelope of the polarization grating has a much slower decay than does the intensity grating, and the polarization-grating decay constant is sensitive to fringe spacing over the same range of spacings. The behavior of the polarization gratings is consistent with diffusionally dominated decay with an additional 6 ns time-constant decay term. This time constant is an order of magnitude longer than the quenching-induced lifetime observed in the intensity-grating decays.

Intensity- and polarization-grating data in low-pressure Na vapor at a fringe spacing of 22 $\mu$m are shown in Figs. 3(a) and 3(b). The $D_1$ transition (at 589.6 nm) was excited and the $D_2$ transition (589.0 nm) was probed. The polarization-grating decays again contain large oscillations, as was the case in the flame. The intensity-grating decays can be shown from electric-field picture considerations to be related to the Fourier transform of the Na velocity distribution[4,5] (as well as the Na excited-state lifetime). At very low pressure (such that the mean free path of a Na atom is greater than a fringe spacing), the velocity distribution is a Gaussian Maxwell–Boltzmann distribution. The intensity-grating decay is given by[5]

$$S(t) \propto \exp[-(\Delta t)^2 k_B T/m]\exp(-2t/\tau), \qquad (6)$$

where $k_B$ is Boltzmann's constant, $T$ is the temperature, and $m$ is the atomic mass. One might imagine that at least the envelope of the polarization-grating decay ought to conform to this expression. While this is true at fringe spacings small enough that transport is the dominant grating decay mechanism, it is not true at larger fringe spacings. The intensity-grating decay from Fig. 3(a) is superimposed on the polarization-grating decay in Fig. 3(b); it can be seen that the two decays differ at long delay times.

Although the electric-field picture can be used to explain the intensity-grating decays, it neither predicts the oscillations nor the insensitivity to excited-state decay of the polarization gratings. Standard DPT can be used to explain the oscillations, but not the decay behavior of the gratings. The GDM provides the additional spatial information necessary for understanding these decays, however.

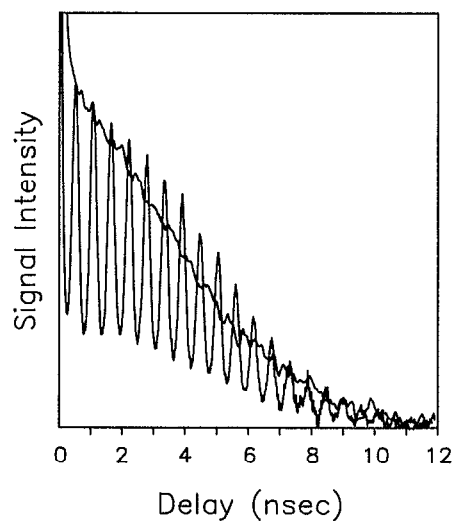


FIG. 3. (a) Linear intensity grating in a low-pressure (collisionless) sodium cell. The fringe spacing is 22 $\mu$m, the excitation wavelength 589.6 nm, and the probe wavelength 589.0 nm. (b) Linear polarization grating in a low-pressure sodium cell under the same conditions as in (a). The decay envelopes are mainly due to the Maxwell–Boltzmann velocity distribution of the Na atoms. The oscillations in (b) are caused by the hyperfine splitting in the Na ground state. The decay in (a) is superimposed on the decay in (b) as a dashed line, to illustrate that the polarization-grating envelope does not correspond to the intensity-grating decay at long decay times. The magnitudes of the two decays were matched at an arbitrary delay time long enough that the coherence artifact does not affect either decay.

The observed effects can be explained in terms of coherences induced in the Na magnetic sublevels by the light fields. An energy-level diagram for Na is given in Fig. 4. Spin–orbit coupling splits the $3p$ orbitals into the $P_{1/2}$ and $P_{3/2}$ levels. Coupling with the nuclear spin, $I = 3/2$, yields the total coupled angular momentum, $F$. Thus, the $S_{1/2}$ ground state and the $P_{1/2}$ excited state are both split into two levels ($F = 1$ and $F = 2$) and the $P_{3/2}$ state is split into four levels ($F = 0$, $F = 1$, $F = 2$, and $F = 3$). Each of these $F$ levels has $2F + 1$ magnetic sublevels, with quantum numbers $m_F = -F$ to $F$.

Since, for the data in Figs. 2 and 3, the excitation and probe wavelengths were tuned to two different excited states, this particular experiment is described by the two "absorption" Feynman diagrams from I. We must still sum over all possible four-wave mixing (FWM) pathways, however; for this we use the absorption ETIMEs ($a$-ETIMEs) for the Na $D_1$ and $D_2$ transitions. It is a property of these particular $a$-ETIMEs that ${}^{ex}M_{ab}(\eta_1,\eta_2) = -{}^{ex}M_{ab}(\eta_2,\eta_1)$, where $\eta_1$ and $\eta_2$ are two orthogonal linear polarizations. As an example, we list in Table I the $a$-ETIMEs for the $D_1$ and $D_2$ lines for $\eta_1 = \mathbf{x}$ and $\eta_2 = \mathbf{y}$ (and vice versa); a full list of the ETIMEs for the Na $D_1$ and $D_2$ lines is given in Ref. 17. Thus, following the argument given in I, we need consider only the circularly polarized component intensity gratings in the analysis of the above experiments. In fact, for the $P_{1/2}$ manifold the stimulated-emission ETIMEs ($e$-ETIMEs) with orthogonal linear polarizations also have the property that they change sign upon interchange of the polarizations (although those for the $P_{3/2}$ manifold do not), so we could apply the same argument if we were exciting and probing the $D_1$ line.

We perform all of our calculations with a laser bandwidth much smaller than the 17 $cm^{-1}$ splitting between the $P_{1/2}$ and $P_{3/2}$ manifolds of states. We consider first the intensity grating, for which there is no decomposition to perform. We approximate the signal pulse as a delta function in time (although we have already assumed that the laser pulse has a finite-frequency bandwidth, there is a large range of pulse lengths for which both approximations can be used simultaneously), so we need only evaluate the sums

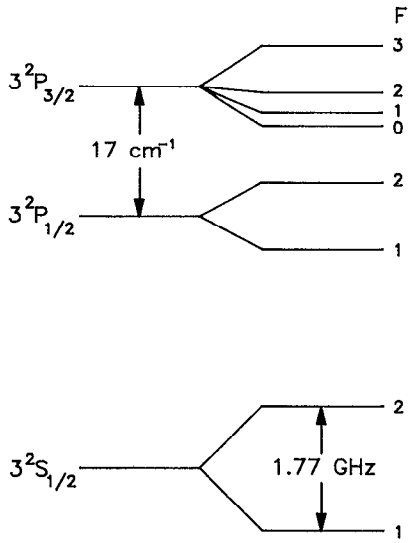


FIG. 4. Energy-level diagram for sodium $3s$ and $3p$ orbitals.

$$\wp^{(3)} \propto \sum_{j,k} E_1 E_2^* E_3 \, {}^{1/2}M_{jk}\{\mathbf{x},\mathbf{x}\} \, {}^{3/2}M_{kj}\{\mathbf{x},\mathbf{x}\} \times \exp(-\Gamma_{jk} t)\cos(\omega_{kj} t), \tag{7}$$

where the superscripts on the $a$-ETIMEs indicate through which excited-state manifold the ground-state sublevels $j$ and $k$ are coupled. For this set of polarizations, the above sum becomes

$$\wp^{(3)} \propto E_1 E_2^* E_3 \exp(-\Gamma_e t), \tag{8}$$

where $\Gamma_e$ is the rate at which population returns to the ground manifold of states through decay from the excited state (as will be explained below).

From Eq. (8) we can see that in neither the low-pressure experiment nor the flame experiment is the signal predicted to contain oscillations at $\omega_{hf}$; this agrees with the observed decays. Although terms containing this frequency do occur in the calculation, each of these terms has a corresponding

TABLE I. Absorption ETIMEs for Na $D_1$ and $D_2$ lines for one $x$-polarized and one $y$-polarized excitation beam.

| | | $-i^{\cdot 1/2}M_{jk}(\mathbf{x},\mathbf{y})$, $i^{\cdot 1/2}M_{jk}(\mathbf{y},\mathbf{x})$, $i^{\cdot 3/2}M_{jk}(\mathbf{x},\mathbf{y})$, $-i^{\cdot 3/2}M_{jk}(\mathbf{y},\mathbf{x})$ | | | | | | | |
|---|---|---|---|---|---|---|---|---|---|
| | $k$ | $\|1\,-1\rangle$ | $\|1\,0\rangle$ | $\|1\,1\rangle$ | $\|2\,-2\rangle$ | $\|2\,-1\rangle$ | $\|2\,0\rangle$ | $\|2\,1\rangle$ | $\|2\,2\rangle$ |
| $j$ | $\|1\,-1\rangle$ | $-1/6$ | | | | $-\sqrt{1/12}$ | | | |
| | $\|1\,0\rangle$ | | | | | | $-1/3$ | | |
| | $\|1\,1\rangle$ | | | $1/6$ | | | | $-\sqrt{1/12}$ | |
| | $\|2\,-2\rangle$ | | | | $1/3$ | | | | |
| | $\|2\,-1\rangle$ | $-\sqrt{1/12}$ | | | | $1/6$ | | | |
| | $\|2\,0\rangle$ | | $-1/3$ | | | | | | |
| | $\|2\,1\rangle$ | | | $-\sqrt{1/12}$ | | | | $-1/6$ | |
| | $\|2\,2\rangle$ | | | | | | | | $-1/3$ |

term that destructively interferes with it. Thus, all of the terms that oscillate at $\omega_{hf}$ cancel. This type of explanation was originally given by Rose *et al.*,[5] but their mathematical argument was a qualitative one that did not accurately describe the experiment as a whole.

We now turn to the polarization-grating calculation. We know from the properties of the *a*-ETIMEs for this system that we can ignore the linearly polarized component gratings in the decomposition. We can make an additional calculational simplification by considering the probing steps. Using the fact that, in the absence of secondary effects such as the OKE, probing a linear intensity grating with linearly polarized light produces a signal of the same polarization as the probe, we can show through a few simple manipulations that the contribution to $\wp^{(3)}$ arising from the LCP component grating is the negative of the contribution to $\wp^{(3)}$ arising from the RCP component grating. However, the two gratings are spatially 180° out of phase, and so they contribute identically to $\wp^{(3)}$ when the probe beam is $x$ polarized and the signal $y$ polarized. Thus, we need consider only the contribution of one of the circularly polarized component gratings in deriving $\wp^{(3)}$. Even if the calculation is performed with normal matrix elements (as opposed to ETIMEs), it is easier to calculate $\{\mathbf{r},\mathbf{r}^*\}$ than $\{\mathbf{x},\mathbf{y}^*\}$, in that there are fewer allowed paths available among magnetic sublevels when using matrix elements for circularly polarized light (this is because the selection rule for $\mathbf{r}$ is $\Delta m_F = +1$, whereas for $\mathbf{x}$ or $\mathbf{y}$ it is $\Delta m_F = \pm 1$).

We can now work through the calculation for the polarization grating, following the methods outlined in I and summing the *a*-ETIMEs over all initial ground-state sublevels. We find that

$$|\wp^{(3)}|^2 \propto |E_1 E_2^* E_3|^2 \times [18\exp(-2\Gamma_g t) + 25\exp(-2\Gamma_{gg'} t) + 60\exp(-\Gamma_g t)\exp(-\Gamma_{gg'} t)\cos(\omega_{hf} t) + 25\exp(-2\Gamma_{gg'} t)\cos(2\omega_{hf} t)], \quad (9)$$

where $1/\Gamma_g$ is the time constant for the recovery of the initial ground-state population distribution, and $1/\Gamma_{gg'}$ is the time constant for the decay of coherences between the ground-state hyperfine levels. Note that we distinguish $\Gamma_g$ in this calculation from $\Gamma_e$, the excited-state decay rate in the intensity-grating calculation. These decay constants are purely phenomenological, and there is no intrinsic reason to believe that they are different based on standard DPT for closed systems. Thus, although standard DPT predicts the smooth intensity-grating decay and the oscillations in the polarization-grating decay, it provides no mechanism for distinguishing the different grating decay mechanisms observed experimentally.

We have so far used the GDM to simplify the perturbative calculation for these experiments. We now illustrate the ability of the GDM to provide physical descriptions that can be used to understand perturbative calculations of orientational grating experiments. In fact, it is possible, using the GDM, to develop a full, qualitative explanation of the behavior of the Na grating decays without doing perturbative calculations. As we will show, this problem can be solved by considering the effects of the four component intensity gratings on the ground-state magnetic sublevels.

We start by noting that a ground-state recovery constant does not really measure the rate of population decay from the excited state, but rather the rate at which the system returns to a state that is indistinguishable from its original state. In the experiments described here, all of the ground-state magnetic sublevels are initially equally populated, because $\hbar\omega_{hf}$ is negligible compared to $k_B T$. Decay of population from the excited state is not necessarily sufficient to return the system to this original state. For instance, the excited state may decay preferentially into particular ground-state magnetic sublevels. Alternately, the grating excitations steps may affect each ground-state magnetic sublevel differently, and these differences in the properties of the magnetic sublevels may not be removed by excited-state decay. We will show with the aid of the GDM that the latter explanation accounts for the observed behavior of the flame gratings, whereas both of the explanations are important in the low-pressure gratings.

Although negligible population transfer is implicit in the perturbative treatment of FWM, we can still calculate the relative amount of population transferred out of each ground-state magnetic sublevel after the excitation pulses. Since we are in the low-power limit, much more population is transferred out of the ground-state levels by the first field intervention than is transferred back from the excited state by the second field intervention. Thus we can approximate that the amount of population transferred out of a given magnetic sublevel is simply the sum of the oscillator strengths between that level and the magnetic sublevels of the excited state. [More rigorously, we might calculate $\rho_{gg}(2)$ for all four-component gratings considering all possible diagrams, including those that do not contribute to the signal; however, such a treatment will give the same result.] Although this is a straightforward calculation to perform for the intensity grating, it is possible to look at the spatial nature of the transfer in the polarization grating only through decomposition into the four component intensity gratings. Figure 5(a) shows the relative populations transferred out of the three $F = 1$ ground-state magnetic sublevels through excitation into the $P_{1/2}$ manifold for both the intensity grating (solid curves) and the sum of the four component gratings of the polarization grating (dashed curves). The differences between the two gratings are striking. In the intensity grating, the population transfer from each of the ground-state magnetic sublevels has both the same spatial dependence and the same amplitude. On the other hand, the magnetic sublevels in a polarization grating have population transfers that differ both in spatial dependence and in amplitude.

The behavior of the ground-state magnetic sublevels in the polarization grating can be understood in terms of optical pumping.[24] Consider, for instance, the $|2\ 2\rangle$ ground-state magnetic sublevel; because the selection rule for transitions driven by RCP light is $\Delta m_F = +1$ and because there is no sublevel in the $P_{1/2}$ manifold with $m_F = 3$, the RCP component intensity grating does not drive any transitions out of this ground-state sublevel. On the other hand, the selection

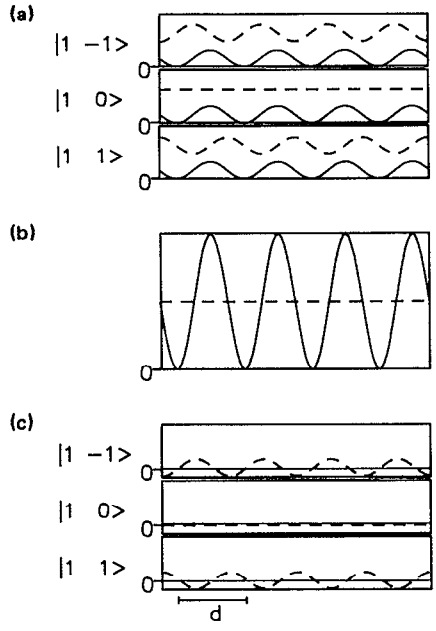


FIG. 5. (a) Spatial dependence of population transferred out of the three magnetic sublevels in the $F=1$ ground-state hyperfine level immediately after excitation. In all plots, the solid lines are for the intensity grating and the dashed lines are for the polarization grating. (b) Spatial dependence of the excited-state population immediately after excitation, under the same conditions as in (a). (c) Spatial dependence of population in magnetic sublevels of $F=1$ ground-state hyperfine level after complete, $m_F$-independent, excited-state quenching.

rule for LCP light is $\Delta m_F = -1$, so there are two magnetic sublevels in the $P_{1/2}$ manifold to which transitions can be driven from this ground-state sublevel by the LCP component intensity grating. Similarly, no transitions are driven out of the $|2\ -2\rangle$ ground-state magnetic sublevel by the LCP component intensity grating, whereas the RCP component intensity grating does drive transitions. Because the LCP and RCP gratings are spatially 180° out of phase, so is the population driven out of the $|-2\ 2\rangle$ and $|2\ 2\rangle$ ground-state magnetic sublevels. In fact, any ground-state magnetic sublevel for which $m_F \neq 0$ is affected differently by the LCP and RCP component intensity gratings. As can be seen in Fig. 5(a) for the $|1\ 0\rangle$ ground-state magnetic sublevel, the population transfer from sublevels with $m_F = 0$ shows no spatial dependence at all, but is instead constant across the grating. This is because, from symmetry considerations, transitions from sublevels with $m_F = 0$ must be driven equally by RCP and LCP light.

Given this understanding of how the grating excitation process affects the ground-state magnetic sublevel populations, we can now describe how collisional quenching and fluorescence contribute to the grating decays. In the flame experiment, where quenching dominates over fluorescence, there is no reason to believe that collisional relaxation events should preserve $m_F$ in any way. Thus, in this experiment we can assume that any excited-state population is quenched with equal probability into each of the ground-state magnetic sublevels. The decays in the low-pressure cell are modeled differently. From the above population transfer calculation, we can also derive the spatial dependence of the population transferred into each of the $P_{1/2}$ magnetic sublevels during the intensity-grating excitation step. Thus, we calculate the effect of fluorescence on each of the initial ground-state magnetic sublevel gratings by considering the oscillator strengths from each of the excited-state sublevels into each of the ground-state magnetic sublevels.

We are now equipped to calculate the effects of both types of population relaxation on intensity- and polarization-grating decays. We first consider collisional quenching. Since we assume that any excited-state population is quenched with equal probability into any of the ground-state magnetic sublevels, we need only consider the spatial dependence of the *total* excited-state population, as opposed to that of the population in each of the excited-state sublevels. In the intensity grating, the $P_{1/2}$ population has the same spatial dependence as (albeit a different amplitude than) the population in each of the ground-state sublevels, as is shown in the solid plot in Fig. 5(b). Collisional quenching therefore fills in each of the ground-state gratings equally. Once all of the population has returned from the excited state, the ground-state gratings have been completely washed out, as is illustrated in the solid plot in Fig. 5(c). Thus, the intensity-grating decay in the atmospheric-pressure flame follows

$$S(t) \propto \exp(-2\Delta^2 Dt)\exp(-2\Gamma_e t). \tag{10}$$

This expression is equivalent to Eq. (5), since $\Gamma_e$ is the inverse of the collisional-quenching time.

Because the electric field in the polarization grating is of constant amplitude across each fringe spacing, the total excited-state population is constant across the grating, as shown in Fig. 5(b). If the population is returned to each ground-state sublevel with equal probability, the depths of the ground-state gratings will not change. Figure 5(c) shows the relative populations of the $F=1$ ground-state sublevels after complete collisional quenching; although the gratings in the $|1\ -1\rangle$ and $|1\ 1\rangle$ sublevels have different offsets after quenching than they did initially, the grating magnitudes are unchanged. Thus, quenching collisions do not contribute to the polarization grating decay.

There are two ground-state phenomena that contribute to the polarization-grating signal, however: the gratings in the sublevels and coherences between sublevels in *different* hyperfine levels (we have chosen a basis set in which there are no coherences between sublevels in the same hyperfine level). The coherences between the hyperfine levels account for the oscillatory term in $\wp^{(3)}$, while the population redistribution among Zeeman levels provides a nonoscillatory term; because the signal is proportional to $|\wp^{(3)}|^2$, beats appear in the data at both $\omega_{\rm hf}$ and at $2\omega_{\rm hf}$. The beats would be expected to be observed only at twice the ground-state hyperfine-splitting frequency if there were no zero-frequency term in $\wp^{(3)}$. Collisions that dephase only the coherences between the hyperfine levels cause only the oscillatory terms to decay. On the other hand, collisions that randomize the ground-state magnetic sublevel populations must also necessarily dephase the coherences, and therefore should cause the both oscillatory and the constant terms to decay. De-

phasing of the hyperfine coherences would not eliminate the signal, but rather would cause the oscillations to damp. Since this is not observed in the flame decays, we conclude that scattering among the hyperfine levels is much faster than the pure dephasing.

Given the above analysis, we may set $\Gamma_g$ equal to $\Gamma_{gg'}$. When quenching is the dominant relaxation process, we obtain

$$S(t) \propto [43 + 60\cos(\omega_{\rm hf}t) + 25\cos(2\omega_{\rm hf}t)] \times \exp(-2\Gamma gg't)\exp(-2\Delta^2 Dt). \quad (11)$$

This expression does an excellent job of reproducing the polarization grating decays in the atmospheric-pressure flame. Note that the 6 ns decay time observed in the polarization grating corresponds to the rate of scattering population among the ground-state magnetic sublevels, $\Gamma_{gg'}$.

Fluorescence affects intensity and polarization grating decays differently than does collisional quenching. In the intensity grating, we calculate that the population transferred into each of the $P_{1/2}$ magnetic sublevels is identical to the population transferred out of each of the ground-state magnetic sublevels. Fluorescence repopulates each of the ground-state magnetic sublevels equally. Once all of the excited-state population has relaxed to the ground state, there are no ground-state gratings left, and therefore no signal. Thus, in a low-pressure Na cell, where there is no collisional quenching and we are in the free-transport regime, the intensity-grating decay will follow

$$S(t) \propto \exp[-(\Delta t)^2 k_B T/m]\exp(-2\Gamma_e t). \quad (12)$$

This is equivalent to Eq. (7), since $\Gamma_e$ is the inverse of the excited-state lifetime, $\tau$. This expression fits the observed decays so long as there is very slow or very fast scattering of population between the $P_{1/2}$ and $P_{3/2}$ levels.[3]

In the polarization grating, the population transferred into a given $P_{1/2}$ magnetic sublevel $|F\,m_F\rangle$ is the same as the population transferred out of ground-state magnetic sublevel $|F\,-m_F\rangle$. For instance, the population transferred into the $|2\ 2\rangle$ excited-state magnetic sublevel has the same spatial dependence as the population transferred out of the $|2\ -2\rangle$ ground-state magnetic sublevel. Subsequent fluorescence from these excited-state sublevels affects the amplitudes of the ground-state sublevel gratings in different manners; some gratings become deeper, whereas others become more shallow. However, fluorescence causes the grating signal to decay by only a few percent, so its effect is small enough that it can be ignored. Thus we approximate for the polarization-grating decay in the low-pressure Na cell

$$S(t) \propto \exp[-(\Delta t)^2 k_B T/m]\,[43 + 60\cos(\omega_{\rm hf}t) + 25\cos(2\omega_{\rm hf}t)]. \quad (13)$$

Note that we have omitted $\Gamma_g$ and $\Gamma_{gg'}$ in this expression, since collisional effects are negligible on the experimental time scale. The low-pressure Na cell polarization-grating decays are fit well by this equation. Comparison with Eq. (12) shows that the envelope of the polarization-grating decay should not conform to the intensity grating when the lifetime decay term is not negligible compared to the velocity distribution decay term.

## IV. CONCLUSIONS

We have illustrated the application of the GDM to two orientational grating problems. In the first example, we used the GDM to augment and add insight to previous treatments of OKE orientational gratings in molecular liquids. Our second example was a specific application of the GDM to a system that cannot be completely described using standard DPT. With the aid of the GDM, we were able to develop a detailed, physical picture that completely describes the behavior of Na intensity and polarization gratings. The qualitative understanding of the important aspects of this problem does not rely on perturbative calculations. These qualitative results are essential to the complete perturbative treatment of the problem. Using the GDM and the symmetry properties of the Na ETIMEs, we were able to greatly reduce the complexity of this calculation and to understand dynamics that would not emerge from a standard DPT calculation.

## ACKNOWLEDGMENTS

This work was supported in part by the Office of Naval Research, Physics Division, Grant No. N000014-89-J1119. R.T. thanks the U.S. Department of Energy, Office of Basic Energy Sciences, Chemical Sciences Division, for support. Computing equipment was provided by the National Science Foundation, Grant No. CHE 88-21737. J.T.F. thanks the National Science Foundation for a graduate fellowship. We wish to thank Dr. Mark Dugan and Dr. Ed Quitevas for critical readings, and Timothy Brewer and Dr. Hackjin Kim for the Na flame data discussed in this paper.[2,3]

[1] J. T. Fourkas, R. Trebino, and M. D. Fayer, J. Chem. Phys. **97**, 69 (1992), preceding paper.
[2] J. T. Fourkas, T. R. Brewer, H. Kim, and M. D. Fayer, Opt. Lett. **16**, 177 (1991).
[3] J. T. Fourkas, T. R. Brewer, H. Kim, and M. D. Fayer, J. Chem. Phys. **95**, 5775 (1991).
[4] T. R. Rose, W. L. Wilson, G. Wäckerle, and M. D. Fayer, J. Phys. Chem. **91**, 1704 (1987).
[5] T. S. Rose, W. L. Wilson, G. Wäckerle, and M. D. Fayer, J. Chem. Phys. **86**, 5370 (1987).
[6] G. Eyring and M. D. Fayer, J. Chem. Phys. **81**, 4314 (1984).
[7] F. W. Deeg and M. D. Fayer, J. Chem. Phys. **91**, 2269 (1989).
[8] E. Hecht and A. Zajac, *Optics* (Addison-Wesley, Reading, MA, 1974).
[9] K. Sala and M. C. Richardson, Phys. Rev. A **12**, 1036 (1975).
[10] J. Etchepare, G. Grillon, J. P. Chambaret, G. Hamoniaux, and A. Orszag, Opt. Commun. **63**, 329 (1987).
[11] K. A. Nelson, R. J. D. Miller, D. R. Lutz, and M. D. Fayer, J. Appl. Phys. **53**, 1144 (1981).
[12] R. J. D. Miller, R. Casalegno, K. A. Nelson, and M. D. Fayer, Chem. Phys. **72**, 371 (1982).
[13] R. Trebino, C. E. Barker, and A. E. Siegman, IEEE J. Quantum Electron. **QE-22**, 1413 (1986).
[14] C. E. Barker, Ph.D. thesis, Stanford, 1988 (unpublished).
[15] K. A. Nelson, J. Appl Phys. **53**, 6060 (1982).
[16] R. W. Hellwarth, Prog. Quantum Electron. **5**, 1 (1977).
[17] J. T. Fourkas, Ph.D. thesis, Stanford University, 1991 (unpublished).
[18] L. J. Rothberg and N. Bloembergen, Phys. Rev. A **30**, 820 (1984).
[19] L. J. Rothberg and N. Bloembergen, Phys. Rev. A **30**, 2327 (1984).
[20] R. Trebino and L. A. Rahn, Opt. Lett. **12**, 912 (1987).
[21] R. Trebino and L. A. Rahn, Opt. Lett. **15**, 354 (1990).
[22] B. P. Kibble, G. Copley, and L. Krause, Phys. Rev. **153**, 9 (1967).
[23] J. R. Barker and R. E. Weston, Jr., J. Chem. Phys. **65**, 1427 (1976).
[24] M. D. Levenson and S. S. Kano, *Introduction to Nonlinear Laser Spectroscopy* (Academic, Boston, 1988).